RESEARCH ARTICLE

Enhanced *in vivo*-imaging in medaka by optimized anaesthesia, fluorescent protein selection and removal of pigmentation

Colin Q. Lischik[1,2], **Leonie Adelmann**[1], **Joachim Wittbrodt**[1] *

1 Centre for Organismal Studies (COS) Heidelberg, Heidelberg University, Heidelberg, Germany,
2 Heidelberg Biosciences International Graduate School, Heidelberg University, Heidelberg, Germany

* jochen.wittbrodt@cos.uni-heidelberg.de

Abstract

Fish are ideally suited for *in vivo*-imaging due to their transparency at early stages combined with a large genetic toolbox. Key challenges to further advance imaging are fluorophore selection, immobilization of the specimen and approaches to eliminate pigmentation. We addressed all three and identified the fluorophores and anaesthesia of choice by high throughput time-lapse imaging. Our results indicate that eGFP and mCherry are the best conservative choices for *in vivo*-fluorescence experiments, when availability of well-established antibodies and nanobodies matters. Still, mVenusNB and mGFPmut2 delivered highest absolute fluorescence intensities *in vivo*. Immobilization is of key importance during extended *in vivo* imaging. Here, traditional approaches are outperformed by mRNA injection of α-Bungarotoxin which allows a complete and reversible, transient immobilization. In combination with fully transparent juvenile and adult fish established by the targeted inactivation of both, *oca2* and *pnp4a* via CRISPR/Cas9-mediated gene editing in medaka we could dramatically improve the state-of-the art imaging conditions in post-embryonic fish, now enabling light-sheet microscopy of the growing retina, brain, gills and inner organs in the absence of side effects caused by anaesthetic drugs or pigmentation.

Introduction

Fish (Zebrafish, *Danio rerio* [1,2]; Medaka, *Oryzias latipes*, [3,4]) have become popular model systems for *in vivo* imaging due to their transparent embryos and their extended genetic toolbox [5,6].

In contrast to the first hours of development, imaging of subsequent stages of development and adult life is obscured by increasing pigmentation and active movements of the growing animals. Thus, the biggest challenge does not reside on the level of instrumentation, but rather within the specimen itself. They need to be tackled to fully exploit the excellent genetic toolbox. Long term lineaging approaches in both species [7,8] will only deliver dynamic data on fate decisions, once these challenges have been addressed.

This requires a systematic comparative analysis to combine the best suited fluorescent proteins *in vivo* with an improvement of the long-term immobilisation/anaesthesia not interfering with the viability of the organisms and approaches to further enhance the transparency of juvenile and adult fish. All three major challenges are addressed below.

So far, the choice of a given fluorescent protein (FP) as a reporter or tag has often been based on a subjective or pragmatic decision, rather than on quantitative comparison identifying the one best suited. In order to address this, we systematically compared a library of widely used green and red FPs and compared their fluorescence intensities during development upon mRNA injection in medaka and zebrafish embryos.

For this purpose, we scored the respective fluorescence intensities over time and assessed whether a given intensity of a FP is determined exclusively by its amino acid sequence or can be further improved by codon optimization.

The second challenge was identifying a suitable means of anaesthesia for *in vivo* imaging of fish. This is necessary since treatment with the standard anaesthetic, Tricaine or MS222, has been shown to result in incomplete anaesthesia accompanied by adverse effects on cardiac development [9]. Together with Tricaine, we systematically tested anaesthesia, induced by the GABA modulating agent Etomidate and α-Bungarotoxin, a potent nicotinic acetylcholine receptor (nAChR) inhibitor.

The third challenge was overcoming the optical obstructions posed by the pigmentation of eye and peritoneum which prevent the efficient imaging of the underlying cells, tissues and organs. The melanin-containing pigments are not only absorbing light, but are also auto-fluorescent and consequently interfering with fluorescence microscopy [10]. Similarly, the light reflecting properties of the iridescent iridophores interfere with deep *in vivo* imaging [10]. Furthermore, leucophores show auto-fluorescence and therefore also interfere with fluorescence microscopy [11]. All three represent a challenge for light microscopy, in particular true for light-sheet microscopy, where the illumination axis is positioned perpendicular to the detection axis [1,2]. Retinal pigmentation completely shields the eye and pigmentation of the head interferes with imaging of the brain or any other cranial structure. The most widely used method to suppress the formation of pigment in developing teleost embryos is the application of the toxic and teratogenic drug 1-phenyl 2-thiourea (PTU) [12]. While PTU prevents formation of new melanin pigment, it neither abolishes already present melanin pigmentation, nor blocks formation of iridophore or leucophore pigment. Consequently, the limited efficacy of PTU towards iridophores and leucophores together with its severe and toxic side effects highlights the need for alternative experimental approaches.

To overcome these limitations large efforts have been made to systematically breed medaka with reduced pigmentation, suitable for *in vivo* imaging [13,14]. However, since these lines were established by combining several different gamma-ray induced mutant alleles affecting pigmentation, the resulting individuals, mutant in five different loci, are severely affected in life span and fecundity and are consequently challenging to maintain [14]. In order to eliminate pigmentation and light reflection in any genetic background without the need for extensive breeding we devised a CRISPR/Cas9-based knockout strategy to establish pigment-free lines in any background by the parallel targeting of pigment formation in melanophores (*oca2* or *tyr*), iridophores (*pnp4a*) and leucophores (*slc2a15b or pax7a*). This highly efficient strategy is even applicable for transient approaches upon microinjection.

Taken together, the combination of the approaches presented in this study (multiple pigment knockout, *α-Bungarotoxin mRNA*, *eGFP* and *H2A-mCherry*) facilitated the imaging of post-embryonic medaka with a MuVi-SPIM (Multiview selective plane illumination microscope) [15,16] highlighting their immediate impact.

Results

mVenNB and mCherry are the most intense fluorescent proteins in medaka

In order to assess the fluorescence intensity of different, commonly used FPs (CFP, Clover, eGFP, eGFPvar, eGFPvarA206K, Venus, YFP, mGFPmut2, mVenusNB, exact fluorophore mutations are listed in S1 Table), we performed a transient ratiometric approach over extended periods of time. To do so we co-injected equimolar amounts of mRNAs encoding the respective green FP along with mRNA encoding mCherry as reference. Embryos were injected at the one-cell stage and placed into a 96 well plate for imaging immediately after injection. We determined green and red fluorescence intensities every 20–33 minutes for at least 40 h at 28°C (exact timeframes are listed in S2 Table, Fig 1C and 1D). We confirmed that the chorion does not negatively impact on the analysis of injected embryos by comparing embryos with and without chorion at 2, 3 and 4 days post fertilisation (dpf) under the conditions detailed above. This analysis showed no interference of the chorion the determination of the fluorescence properties (Fig 1F, S1 Fig).

Subsequently, embryos were demounted and image data were analysed in a semi-automated manner by Fiji and R scripts (Fig 1A). In brief, we determined the fluorescence intensities by first automatically segmenting the outline of the embryo, followed by the extraction of the mean, median and standard deviation of the resulting region of interest defined by the embryonic outline. The values were normalized to the mean value of the reference mCherry fluorescence intensity at 10 hours post fertilization (hpf). For red fluorescent proteins (mCherry, mRFP, mRuby2, tagRFP, mRFP1*, mScarlet-I, exact fluorophore mutations can be found in S1 Table), we used eGFP as ratiometric reference and performed an analogous analysis. The resulting fluorescence intensities at 10 hpf were ordered allowing instant comparison (Fig 1B). Our systematic analysis revealed that mVenNB and mCherry show the highest fluorescent intensities *in vivo* at 10 hpf (Fig 1B). We validated particularly high and low scoring candidates by high resolution imaging of mRNA injected embryos at 8dpf in a selective plane illumination microscope (SPIM) (Fig 1E). This analysis confirmed the initial assessments and underscores the impact of autofluorescence of pigment cells.

Previously Balleza and colleagues compared *in vitro* parameters to *in vivo* fluorescence in *E. coli* in order to identify parameters predictive for *in vivo* fluorescence [18]. In order to assess whether this holds also true for vertebrate systems we compared the fluorescence intensities obtained for the different FPs above to their results (Fig 2A). Most FPs show a similar relative fluorescence intensity compared to the normalization value in *E. coli* and *O. latipes*. However, some particularly intense fluorescent proteins such as *mCherry* and *mVenNB* are prominently diverging from the predicted parameters, underpinning the need of an *in vivo* assay to validate novel FPs in the model organism of choice. Similar findings were reported from *C. elegans*, where the *in vitro* parameters are not a sufficient predictor for *in vivo* fluorescence [19].

We addressed a potential impact of protein structure or codon usage on the fluorescence intensities. We first plotted the codon adaptation index (CAI) [20] for medaka and for human for each of the FP sequences used (Fig 2B). To address the question experimentally, we designed codon optimized eGFP for medaka (OleGFP) by OPTIMIZER [21] and plotted its CAI along with the CAI for an eGFP codon optimized for *Saccharomyces cerevisiae* (SceGFP, Fig 2D). For experimental validation, both mRNAs were injected into medaka embryos, each together with *mCherry* mRNA as injection control and compared to an *eGFP* mRNA control injection. Analysis was performed as described above (Fig 1A). The results indicate that codon averaging does not improve the fluorescence intensity. In contrast, the fluorescence intensity of OleGFP is even lower than that of SceGFP, hinting at inefficient translation in case of the
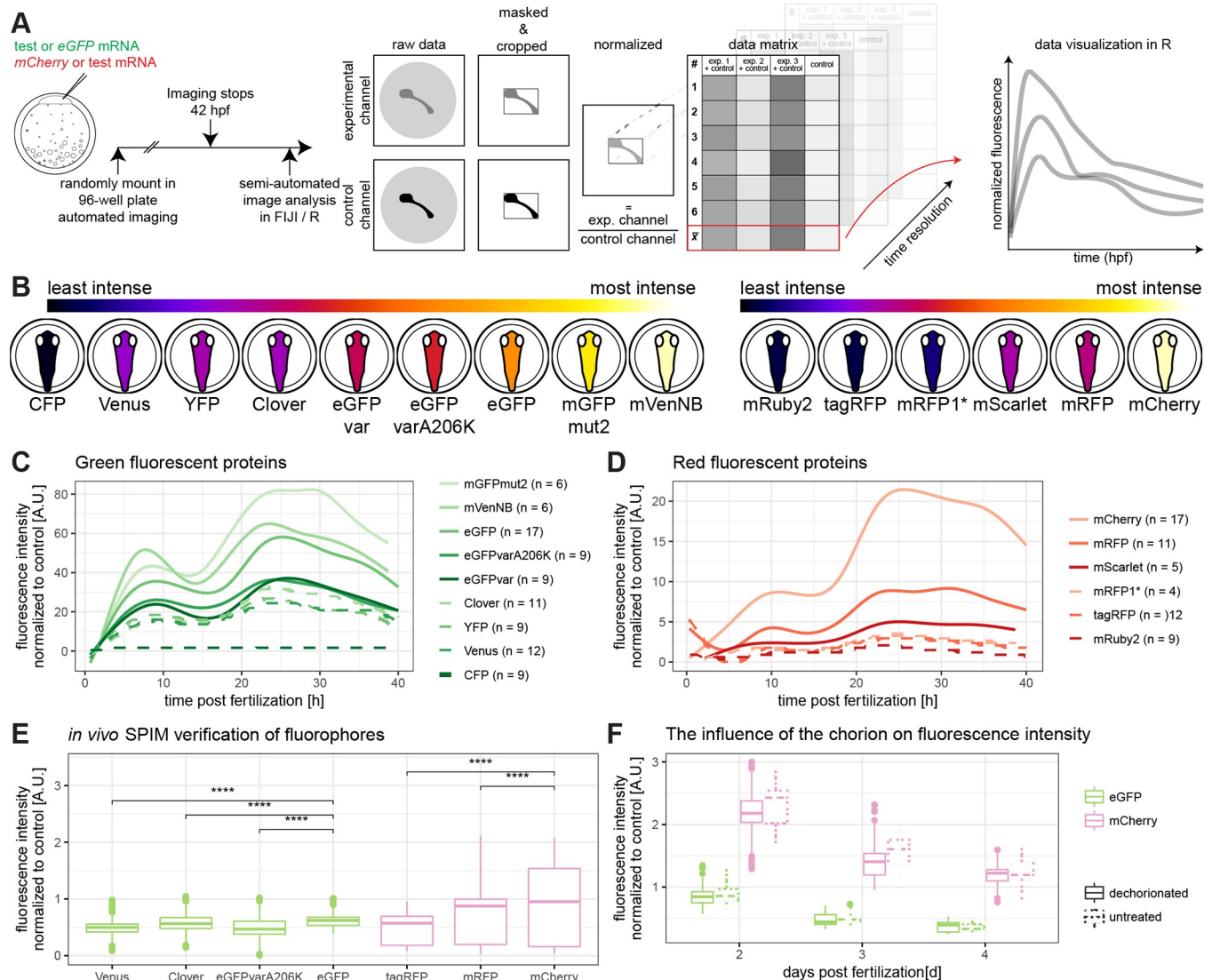
Fig 1. The brightest fluorescent proteins tested in medaka are mVenusNB in the green channel and mCherry in the red channel. (A) Embryos were injected with a green fluorescent protein mRNA to be tested and mCherry mRNA or with eGFP mRNA and a red fluorescent protein mRNA to be tested (1-cell stage modified from [17]). Embryos were mounted in a 96-well plate immediately after injection and automatically imaged for at least 40 h. These data were analysed semi-automated in Fiji and R. Therefore, the raw data were masked and cropped to exclude background. Subsequently, the injection volume was normalized per well by dividing with the value of the control channel at 10 hours post-fertilization. These values were plotted along their biological replicates in R. (B) Schematic overview of fluorescence intensity at 10 hpf, ordered by fluorescence intensity. The lookup table is indicated on the top of the panel, the green fluorescent proteins are shown on the left hand side and the red fluorescent proteins are shown on the right hand side (embryos modified from [17]). (C) Green fluorescent protein fluorescence comparison over time. Plotted is the fluorescence normalized to mCherry per well against the hours post fertilization. Plates were normalized by internal control for fusion of graphs (eGFP). n values indicate number of embryos used for each measurement. (D) Red fluorescent protein fluorescence comparison over time. Plotted is the fluorescence normalized to eGFP per well against the hours post fertilization. Plates were normalized to internal control for fusion of graphs (mCherry). n values indicate number of embryos used for each measurement. (E) Verification of previous results by *in vivo*-microscopy of hatched medaka embryos (8dpf) in a light-sheet microscope, comparing the fluorescence intensity of different fluorescent proteins (asterisks indicate P-values: **** P < = 0.0001, *** P < = 0.001, ** P < = 0.01, * P < = 0.05, ns P > 0.05, Venus N = 3 n = 1483, Clover N = 3 n = 1294, eGFPvarA206K N = 3 n = 1395, eGFP N = 2 n = 794, tagRFP N = 3 n = 1580, mRFP N = 3 n = 2158, mCherry N = 2 n = 980, N indicates number of fish, n indicates number of z-slices used for analysis). (F) The influence of the chorion on fluorescence intensity. Exemplary shown are eGFP and mCherry. There is a negligible influence of the chorion of fluorescence intensity measurement. Further information can be found in S1 Fig.

OleGFP mRNA in comparison to eGFP mRNA (Fig 2C). Taken together, those experiments and the overall similar temporal intensity patterns of all FPs assayed are reflecting a comparable translation regulation of the different mRNAs and comparable stability of the injected
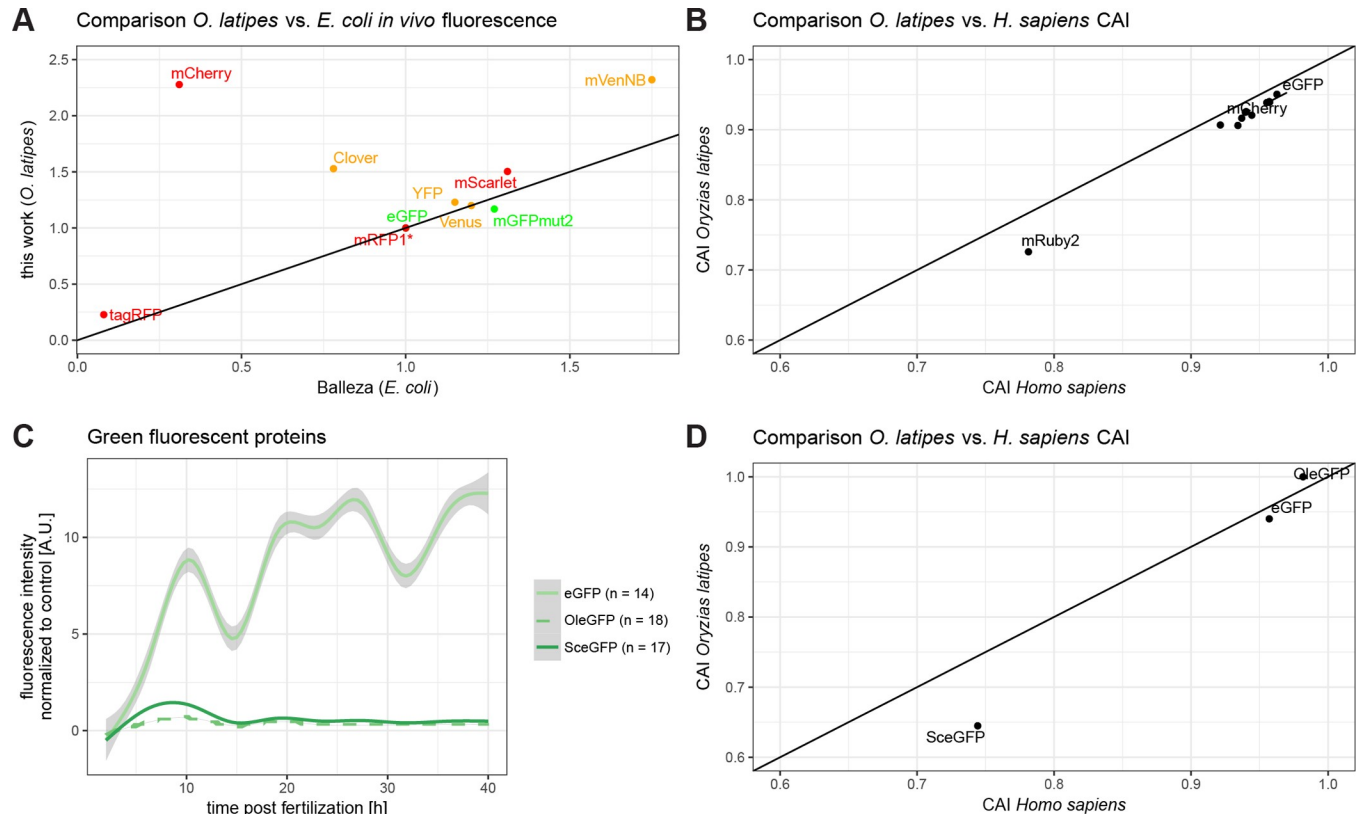
Fig 2. Codon adaptation of *eGFP* for medaka is not improving fluorescence. (A) Relative comparison of *in vivo* fluorescence in medaka with *in vivo* fluorescence in *E. coli*. Indicated are red, green and yellow fluorescent proteins and a diagonal line for orientation. The red, green and yellow fluorescent proteins have been normalized to the same relative values published of mRFP1*, eGFP and Venus, respectively [18]. While many of the fluorescent proteins have similar properties, some are significantly different, reinforcing the need of a systematic review of fluorescent proteins in medaka. (B) Codon adaptation indices (CAIs) of all prior used sequences. Codon adaptation index of each sequence is plotted for medaka and human along with a diagonal line for orientation. Labelled are the two normalizing fluorescent proteins eGFP and mCherry, and the outlier mRuby2. For a plot with full labelling, refer to S2 Fig. (C) Pure codon usage table driven codon averaging does not improve fluorescence intensity of fluorescent proteins. OleGFP (medaka codon-averaged eGFP) fluorescence intensity is overall lower than SceGFP (yeast codon-averaged) and 25 to 30-fold lower than eGFP. (D) Codon adaptation indices of sequences used in order to score for the effect of codon averaging. Additional to the prior used sequences are an eGFP codon optimized for medaka (OleGFP) and an eGFP codon optimized for yeast (SceGFP).

mRNAs respectively (Fig 1C and 1D). Codon optimization does not additionally improve the respective fluorescence properties.

The most intense fluorescent proteins in medaka were also tested in zebrafish and analysed accordingly. Embryos were visualized by the mean over all timepoints, since the trend was not persistent over time (Fig 3A). Green fluorescent proteins (Fig 3B) and red fluorescent proteins (Fig 3C) were normalized to control injections and visualized over time. Strikingly and in contrast to medaka, the trend is not persistent for all FPs, but fluorescence intensity ratios vary with time. So, the time of the assay is of crucial importance for the choice of the optimal FP during early zebrafish development.

α-Bungarotoxin mRNA injection most efficiently anesthetises medaka embryos

To improve the quality of anaesthesia in medaka, different forms of anaesthesia were compared by scoring movements over time. We either treated embryos with the established anaesthetic Tricaine, Etomidate or injected one cell stage embryos with mRNA encoding α-
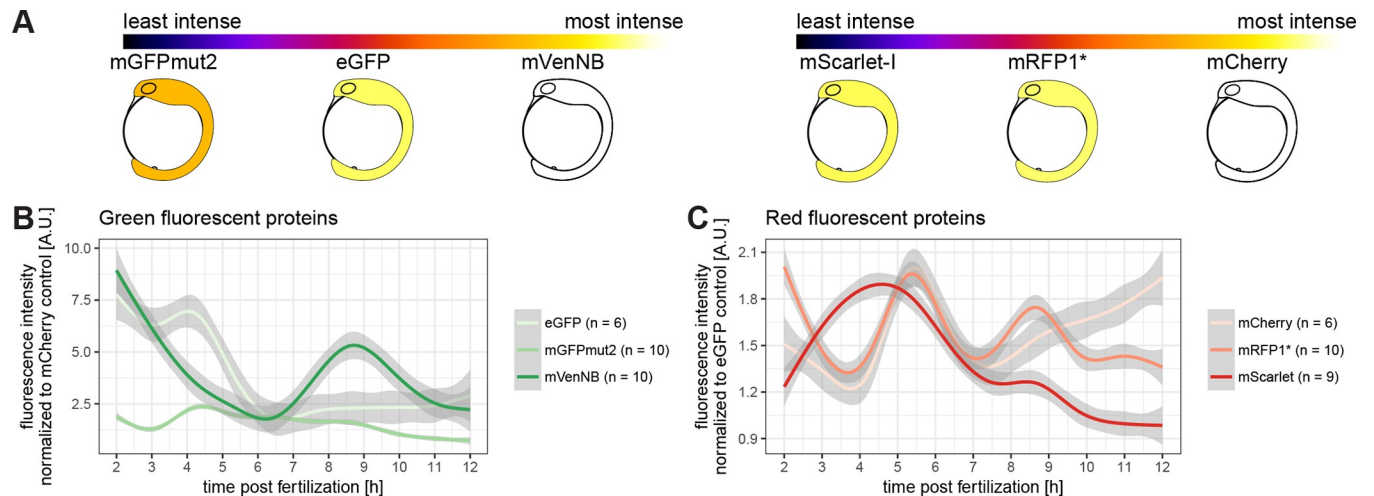
Fig 3. The most suitable fluorescence intensity in zebrafish varies during development. (A) Schematic overview of the mean of the tested fluorescent proteins. The lookup table is indicated at the top of the panel, the green fluorescent proteins are shown on the left hand side and the red fluorescent proteins are shown on the right hand side (embryos modified from [22]). (B) Green fluorescent protein fluorescence comparison over time. Plotted is the fluorescence normalized to mCherry per well against the hours post fertilization. Analysis was conducted as outlined in Fig 1A. (C) Red fluorescent protein fluorescence comparison over time. Plotted is the fluorescence normalized to eGFP per well against the hours post fertilization. Analysis was conducted as outlined in Fig 1A.

Bungarotoxin [23]. All embryos were dechorionated at stage 28 [17], when uninjected embryos were treated with Tricaine, Etomidate, and the respective controls (1xERM, DMSO). To avoid position effects in the 96-well plate, embryos were loaded randomly and imaged in 20 minute intervals for up to 40 hours. To detect movements, we performed semi-automated image analysis in Fiji [24] and R [25] (Fig 4A). Our analysis workflow delivered a quantitative readout of embryonic movement assessing the efficacy of the anaesthetics (Fig 4B). Strikingly, α-Bungarotoxin was the only anaesthetic efficiently blocking embryonic movement. In contrast, Tricaine and Etomidate did not anesthetize efficiently and treated embryos exhibited strong movements over time (Fig 4B, S1 Movie). Importantly, *α-Bungarotoxin* mediated anaesthetics was partially reversible and embryos demounted after the analysis eventually showed startle responses, comparable to that of the control treated groups (Fig 4C). In an injection of 25 $\frac{ng}{\mu l}$ this anaesthesia will last up to 10 days. Taken together, these results indicate that only *α-Bungarotoxin* functions as effective anaesthetic over extended periods of time. To assess the optimal concentration for reversible anaesthesia suitable for imaging that ensures proper embryonic development, we performed microinjections with different concentrations of *α-Bungarotoxin* (Fig 4D). We determined effective concentrations that are functional even for sensitive lines with limited fecundity facilitating ongoing development and breeding for microscopy. In addition we addressed potential effects on cardiac functionality [23], and carefully assayed heart morphology and function after extended imaging in demounted embryos (S3 Fig). Only embryos injected with *α-Bungarotoxin* exhibited normal cardiac function and development, in contrast to the Etomidate or Tricaine treated embryos where heart function was clearly affected by the treatment (S3 Fig).

Efficient CRISPR/Cas9-based pigment ablation in the injected generation

We employed the CRISPR/Cas9-system in medaka embryos [26] to eliminate pigmentation already in the injected generation (F0). We co-injected mRNA encoding Cas9 together with sgRNAs targeting a key gene for melanin formation and carotenoid deposition in
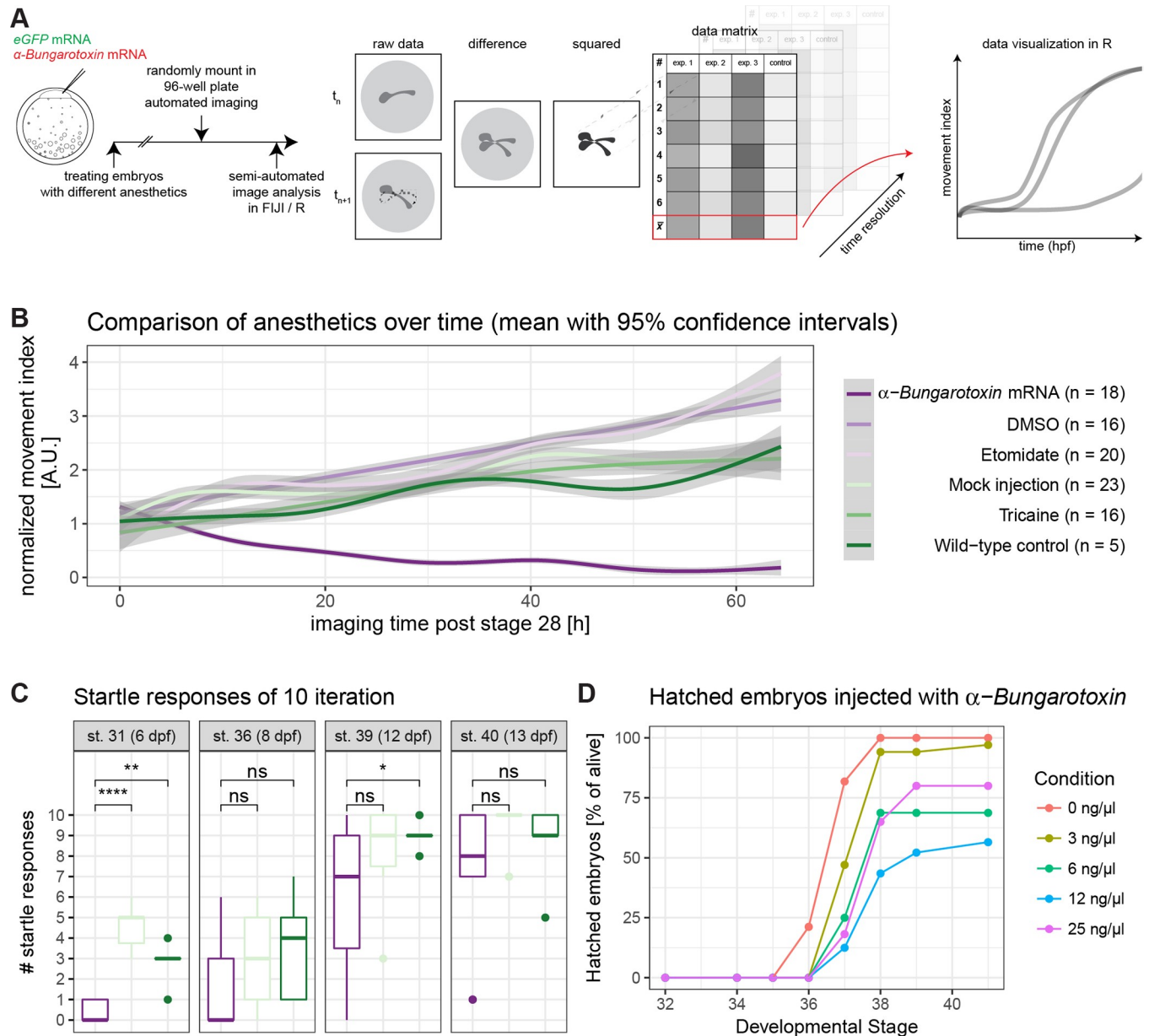
Fig 4. Anaesthesia of medaka is most efficient with α-Bungarotoxin mRNA injection. (A) Embryos were injected with *eGFP* mRNA or *eGFP* mRNA along with *α-Bungarotoxin* mRNA (1-cell stage modified from [17]). Injected embryos and uninjected embryos were dechorionated. Uninjected embryos were treated with Tricaine, Etomidate (experiments), DMSO or 1x ERM (controls). Embryos were randomly loaded in a 96-well plate and imaged automatically. Plates were adjusted by starting stage of imaging and fused into one dataset. Consecutively, image analysis was performed semi-automatically in FIJI and R. Therefore, the difference between each timepoint *n* and its following timepoint *n+1* was calculated and squared. These values were imported into R and plotted along with their biological replicates. (B) Movement index of injected/treated embryos over time. Data was analysed as described in A. Strikingly, only α-Bungarotoxin is completely anesthetizing the embryos leading to nearly no detectable difference between the different timepoints (time resolution: 20 min, n as fish per condition is indicated in the legend). (C) α-Bungarotoxin-treated embryos are catching up in startle response ability. Fish were startled 10 times each and the number of responses was noted. Same legend as in Fig 4B applies. (α-Bungarotoxin: n = 12 fish, mock injected: n = 5 fish, wild-type control: n = 8 fish, asterisks indicate P-values: **** $P < = 0.0001$, *** $P < = 0.001$, ** $P < = 0.01$, * $P < = 0.05$, ns $P > 0.05$). (D) Different dilutions of α-Bungarotoxin were tested in order to adjust the concentration so fish would wake up after microscopy. Embryos were injected with 0, 3, 6, 12 or 25 ng/μl α-Bungarotoxin mRNA along with eGFP mRNA as an injection control. The number of hatched embryos per condition was scored (0 ng/μl: n = 33 fish, 3 ng/μl: n = 34 fish, 6 ng/μl: n = 16 fish, 12 ng/μl: n = 24 fish, 25 ng/μl: n = 22 fish).

https://doi.org/10.1371/journal.pone.0212956.g004

xanthophores *Oca2* [27]. In addition we targeted Tyrosinase (*Tyr*), a key gene for melanin formation [28]. We addressed the formation of light reflective iridophores by targeting *Pnp4a* [29]. To interfere with leucophore pigment formation, we targeted *Pax7a* or *Slc2a15b* [11]. The exact composition of the injection mixes is listed in Table 1. We subsequently scored for imaging suitability as depicted in Fig 5A. *Oca2*, *Pnp4a* and *Tyr* sgRNA-injected embryos were assessed in the bright field, whereas *Pax7a* and *Slc2a15b* sgRNA-injected embryos were assessed in the green fluorescence channel. The determined values were plotted and are shown in Fig 5B. The immediate imaging suitability in F0 can be as high as 78%, depending on the targeted gene and injection mix.

Highest efficiency is obtained by employing more than one sgRNA for each gene to be targeted [30]. Following that strategy the efficiency of establishing embryos completely lacking pigmentation is increased from 12% (Fig 5B, op_1)to 77% (Fig 5B, op_2) underscoring the validity of the approach. op_1 and op_2, differ in the number of sgRNAs targeting different positions within the loci, but not in the targeted loci.

The targeting of *Oca2* or *Tyr* results in comparable frequencies of pigment loss. Similarly, the targeting of *Pax7a* or *Slc2a15b* produces comparable rates of leucophore (auto-fluorescent) free embryos (Fig 5C). The established mutants are fully viable and breed successfully, resulting in translucent embryos and young fish (Fig 5D, S2 Movie). We named the Oca2, Pnp4a double mutants *spooky*, due to the near-invisibility in petri dishes. These pigment-free fish are amenable to whole mount imaging from embryonic stages up to young adults (S4 Fig). The loss of obstructing pigments in the eye facilitates imaging of the brain by light-sheet microscopy. We combined all approaches described above, injected mRNA encoding the most efficient fluorophores (*eGFP* and *H2A-mCherry* mRNA) into *spooky* mutant fish (*Oca2*$^{-/-}$, *Pnp4a*$^{-/-}$) anesthetized with α-Bungarotoxin and performed long-term imaging of retinal and brain structures previously obstructed by pigmentation (Fig 6). The results obtained underscore the importance of combining all approaches related to the specimen to move whole mount *in vivo* imaging to new frontiers.

Discussion

In medaka there is a clear trend of fluorescence intensity, which is maintained throughout the imaging time, i.e. ratios between fluorescent proteins remain stable. This allows for the scoring of fluorescent proteins by fluorescence intensity.

The GFP derived fluorescent proteins mVenNB and mGFPmut2 are ranking highest in fluorescence intensity. The most popular and standard fluorescent protein, eGFP, with a considerable toolset available including antibodies, nanobodies, split-GFP, etc. [31–33] only scores number three with respect to fluorescence intensity. Since the eGFP toolset is likely also

Table 1. sgRNA assembly for the different injection mixes.

	oca2			pnp4a			tyr		pax7a			slc2a15b	
mix	1	2	3	1	2	3	1	2	1	2	3	1	2
op_1	x	x		x									
op_2	x	x	x	x	x	x							
o	x	x	x										
t							x	x					
p									x	x	x		
s												x	x
ops	x	x	x	x	x	x						x	x

https://doi.org/10.1371/journal.pone.0212956.t001
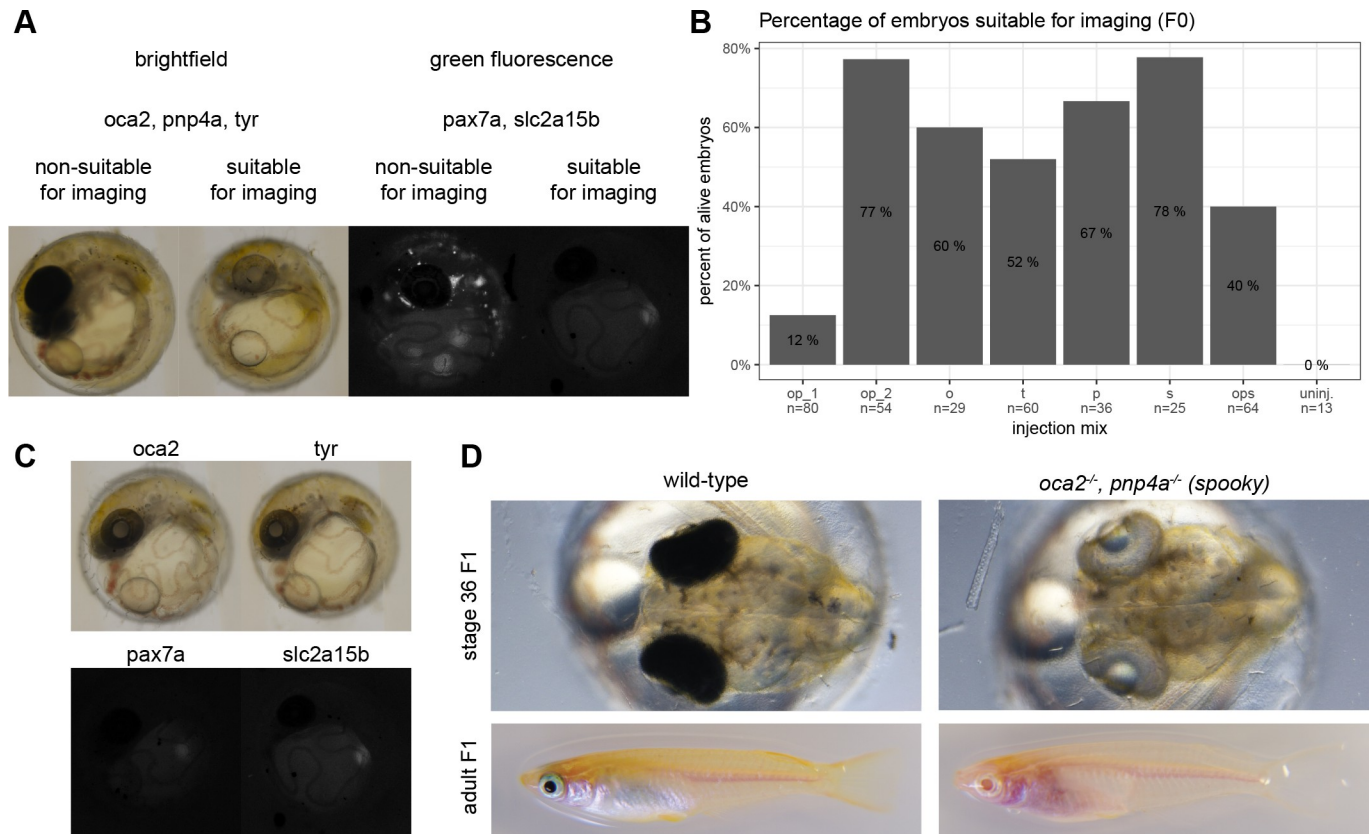
Fig 5. The acute double pigment knockout utilizing the CRISPR/Cas9-system can be deployed in the injected generation. (A) Medaka zygotes were microinjected with Cas9 mRNA and an injection mix according to Table 1. The injected embryos were scored for suitability for imaging either in the brightfield or in the green fluorescent spectrum. The ratio of the embryos suitable for imaging was determined and noted in panel B. (B) Transient targeting efficiency depends on the number of sgRNAs per gene. Compare op_1 and op_2. (C) By visual inspection no difference in pigmentation is observed between *Oca2*⁻/⁻ or *Tyr*⁻/⁻, as well as *Pax7a*⁻/⁻ *Slc2a15b*⁻/⁻ embryos. (D) Medaka injected with the mix op_1 were raised, screened and imaged in F1 to compare the effects of sgRNA injection to wild-type. Wild-type embryos exhibit a dense, black pigment in the eyes, whereas adults additionally exhibit a non-translucent peritoneum. Fish injected with sgRNAs against *oca2* and *pnp4a* show dramatic loss of pigmentation surrounding the eye and the peritoneum, rendering the fish more accessible for microscopy.

applicable to mVenNB and mGFPmut2, the balance between necessary tools and absolute fluorescence intensity will determine the final choice. In some instances, optimization and evaluation could be done *in silico* assessing e.g. antibody binding sites or *in vitro* by immunostaining with antibodies or nanobodies. In addition, the establishment of split fluorescent proteins may be possible. Furthermore, both fluorescent proteins carry an A206K mutation, preventing dimerization making those more amenable for fusion proteins [34]. In conclusion, eGFP remains a solid choice if the experiment heavily relies on secondary factors, which are not entirely based on *in vivo* fluorescence readout.

Among the red fluorescent proteins the number one candidate in medaka is mCherry, which is not only the fluorescent protein with the highest fluorescence intensity, but also with the best established toolbox such as nanobodies, antibodies, etc. [35].

Interestingly, when comparing the measured fluorescence intensities to the theoretical values such as quantum yield and excitation efficiency [36], we observed a discrepancy between measured values and expected results. This might be due to the different physiological conditions inherent to each model organism or underlying non-optimal excitation of fluorescent proteins by single wavelengths.
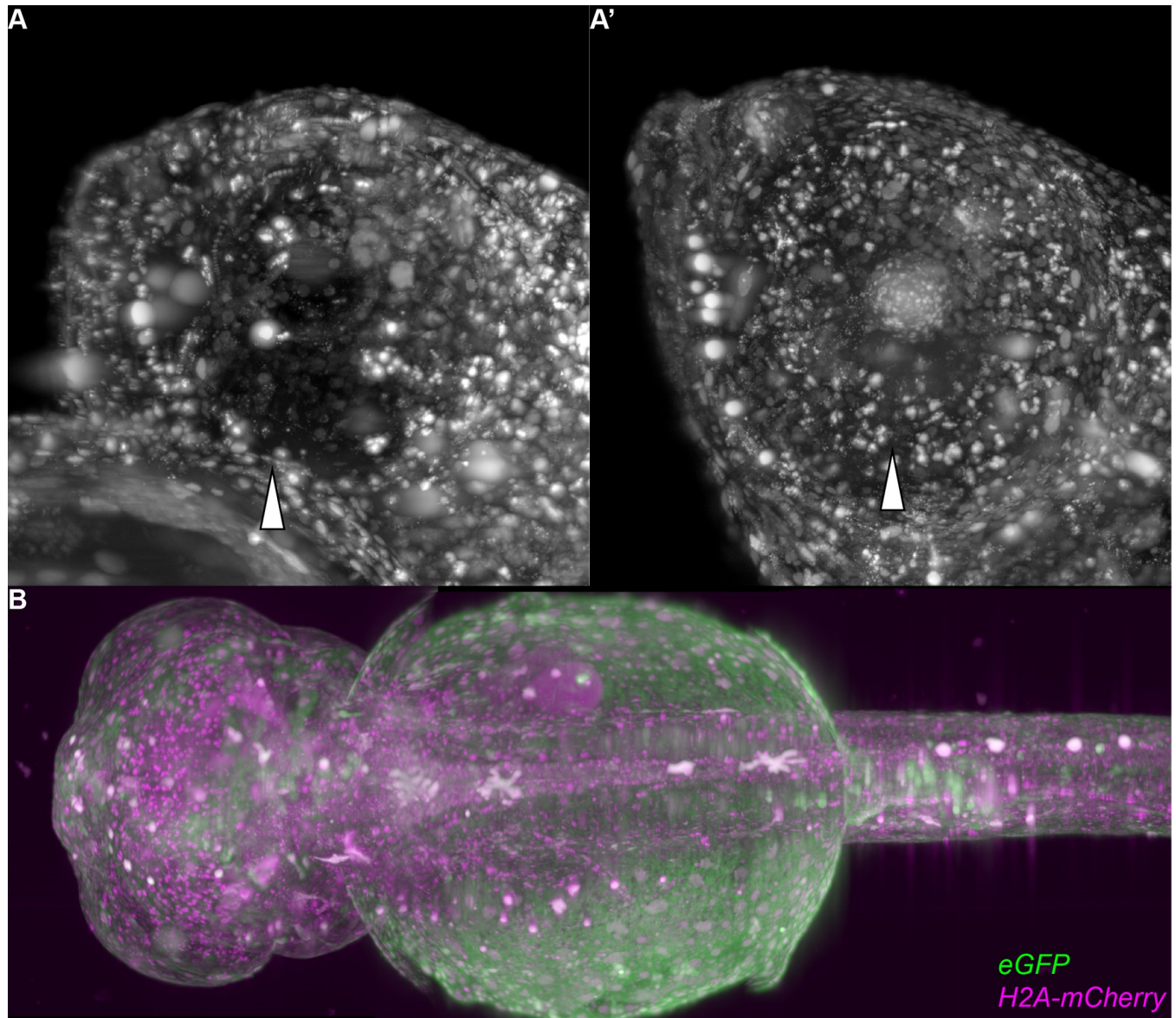
Fig 6. The established toolbox enables imaging of previously challenging organs and tissues, such as the retina and the brain. Using the pigment double knockout in combination with α-Bungarotoxin, eGFP and mCherry coupled to histone2a the imaging was conducted in a single plane illumination microscope (SPIM) we could image the head region of wild-type and *spooky* embryos. Hollow arrowheads point towards the eyes in A and B. (A) Maximum projection of *H2A-mCherry* signal of a lateral view of a wild-type medaka embryo. The eye is not penetrable and no nuclei are visible within or behind it. (A') Maximum projection of *H2A-mCherry* signal of a lateral view of a *spooky* medaka embryo. The eye is penetrable and nuclei are visible within or behind it. (B) Stitched maximum projections of a dorsal view of a *spooky* embryo. This embryo was imaged for 48 hours, which can be seen in S3 Movie.

https://doi.org/10.1371/journal.pone.0212956.g006

Verification of fluorescent proteins by light-sheet microscopy [1,37] is in line with previous observations. Green fluorescent proteins do differ in contrast to more prominent differences among the red fluorescent proteins. Notably, after mRNA injection fluorescence intensity steadily decreases during development, partially accounting for the small distribution of values. It is important to consider that in transgenic lines or after endogenous tagging by CRISPR/Cas9, the most intense fluorescent proteins are continuously expressed and therefore exhibit their fluorescence intensity and maturation time.

The optimal fluorescent protein in zebrafish is not as easy to score by fluorescence intensity. This is due to varying intensities depending on fluorescent protein and developmental stage of the fish. Here, the choice of the optimal fluorescent protein depends on the experimental condition, including the stage of embryos at the time of analysis. Given that we employed standard cassettes ensuring comparable mRNA stability, this may be due to different kinetics of protein maturation and turnover, affecting the quantitative measurements.

Strikingly, most fluorescent proteins show similar *in vivo* fluorescence after normalization in medaka and *E. coli*. However, some of the tested proteins diverge from this trend, reinforcing the need for testing novel fluorescent proteins specifically in the species of choice. Species specific differences may arise from differences in their translational or maturation machinery, cellular pH-values or any combination of components different between the cells of both species.

In our hands the optimization of codon usages according to establish codon usage tables does not improve, but rather decreases fluorescence intensity. It had been shown previously in *Ciona intestinalis* that codon averaging can positively impact on the fluorescence intensity of fluorescent proteins [38]. Our results, in contrast, show that codon-usage table driven averaging is not effective in improving fluorescence intensity, and rather decreased intensity by 25- to 30-fold likely due to changes in mRNA stability or translation efficiency due to repetitive codons.

Even though widely used for fish, the anaesthetic MS222 (Tricaine) has several drawbacks such as non-complete anaesthesia and developmental cardiac defects during extended *in vivo* imaging [9]. Several groups were therefore trying to supplement Tricaine with different anaesthetics such as Isoflurane [39], Etomidate [40] or increasing the dosage of Tricaine itself [41]. The injection of α-Bungarotoxin as alternative approach has previously been suggested for zebrafish, with apparent influence on development or heart morphology [23]. An obvious concern in long-term imaging experiments is the photostability of the anaesthetics. Since α-Bungarotoxin is delivered as an mRNA, the resulting protein is already at the site of action and will be resynthesized proportional to the amount of initially injected RNA, the number of cell division and the stability of the injected mRNA. The ultimate choice of the anaesthetics to be employed finally depends on the biological process to be studies. If those are affected by α-Bungarotoxin, irreversibly binding to nicotinic acetylcholine receptors [23], Tricaine blocking the sodium channels in neuronal membranes [42] or Etomidate potentiating GABA-receptors in the central nervous system [43] might be valid alternatives with limitations discussed above.

The pigment double knockout *spooky* is a valuable addition to toolbox since it is readily established in any existing transgenic of mutant background overcoming time consuming complex breeding schemes to re-establish the transparency of e. g. see-through medaka, homozygously mutant for 5 loci. Already the injected generation facilitates instant deep imaging, most efficiently when more than one sgRNA is selected per locus [30].

The approaches presented here facilitate efficient and deep long-term, *in vivo* imaging of fish embryos and juveniles employing fluorophores with the at best quantum yields in steady, highly transparent embryos e. g. by light-sheet microscopy (Fig 6). We present a streamlined strategy for the optimization of additional species-specific fluorophores and provide cross-validated reference points for immediate comparison of new fluorophores developed.

Materials and methods

Fish husbandry and microinjections, ethics statement

Medaka (*Oryzias latipes*) and zebrafish (*Danio rerio*) stocks were maintained as previously described [44]. The work presented does not involve work with animals according to German

and European legislation. All experiments have been performed at stages prior to the legal onset of animal life. For the generation of those early stages, fish were maintained in closed stocks at Heidelberg University. Medaka (Oryzias latipes) and zebrafish (*Danio rerio*) husbandry and experiments are under the institutional control of the Universities animal welfare agency. Fish were maintained according to local animal welfare standards (Tierschutzgesetz §11, Abs. 1, Nr. 1, husbandry permit number 35–9185.64/BH Wittbrodt) and in accordance with German and European Union animal welfare laws. The fish facility is under the supervision of the local representative of the animal welfare agency. Embryos of medaka of the wildtype Cab strain were used at stages prior to the legal onset of animal life and consequently are not considered animal experiments. Medaka were raised and maintained as described previously. Lines used in the study were medaka wildtype Cab.Embryos were staged according to Iwamatsu [17]. Medaka microinjections were performed as previously described [3].

CRISPR/Cas9 and single guide RNAs

JDS246 was a gift from Keith Joung (Addgene plasmid # 43861). Cas9 mRNA was transcribed by mMessage mMachine Sp6 Transcription Kit (Thermo Fisher). Single guide RNAs were predicted by CCTOP [26] and subsequently cloned into DR274 [45]: sgRNA(Oca2_1): GAAACCC AGGTGGCCATTGC, sgRNA(Oca2_2): TTGCAGGAATCATTCTGTGT, sgRNA(Oca2_3): TGAA CTGGAAGGCTTGTTGC, sgRNA(Oca2_4): GATCCAAGTGGAGCAGACTG, sgRNA(Pnp4a_1): CCTGGGGGCGGTGCTTAGTC, sgRNA(Pnp4a_2): GGAGGGCGTCTACGCCATGG, sgRNA (Pnp4a_3): CATCATCTGTGGCTCTGGAC, sgRNA(Pax7a_1): GGTAATTCTGGCCTGGCGCA, sgRNA(Pax7a_2): AAGGGCTCGGTGGCGTAAGC, sgRNA(Pax7a _3): GAGGAGTGTTCATCAA CGGG, sgRNA(Slc2a15b _1): CGCTCCGGTCATCCCGCCGA, sgRNA(Slc2a15b _2): CAGGTAAC AATAAGGACCCG, sgRNA(Tyr _1): TATCCAGACAAATAGGTCGT, sgRNA(Tyr _2): GTACGT GGGTAGATGGACCG. DR274 was a gift from Keith Joung (Addgene plasmid # 42250) [45]. The vector was linearized by DraI-digest and transcribed by MEGAscript T7 transcription Kit (Thermo Fisher). All RNAs were purified by RNeasy Mini Kit (Qiagen). Injected concentrations were: 150 ng/µl Cas9 mRNA and 15 ng/µl per sgRNA.

Loading and imaging of 96-well plates

96-well plates were loaded with 150 µl volume per well, including the treatment solution and the embryo. The plates were loaded based on a randomized loading scheme created by a customized R script, which creates a loading scheme and a table of each well for further use in the analysis. The plates were sealed by a gas permeable moisture barrier seal (4ti-0516/96, 4titude, Dorking, England), loaded into the ACQUIFER Imaging Machine (DITABIS, Pforzheim, Germany) and imaged for a defined time and channel composition. The plates were continuously incubated at 28˚C. An overview of the imaged plates can be found in S2 Table along with the timeframe, timestep and used channels. A general description of the imaging condition can be found in the section about the semi-automated analysis of the experiment, i.e. either anaesthetic or fluorescent protein analysis.

The used LEDs and filters in the ACQUIFER Imaging Machine were a 470 nm LED in combination with LED-FITC-A-000 (Semrock, Inc.) for the green channel and a 550 nm in combination with a LED-TRITC-A-000 (Semrock, Inc.) for the red channel.

Anesthesia reagents

α-Bungarotoxin mRNA was transcribed from pmtb-t7-alpha-bungarotoxin, which was a gift from Sean Megason (Addgene plasmid # 69542) [46]. The vector was digested by EcoRV-digest and the linearized plasmid transcribed by mMessage mMachine Sp6 Transcription Kit

(Thermo Fisher) for 4h. The mRNA was purified with the RNeasy Mini Kit (Qiagen). Embryos were microinjected with 3–25 ng/µl α-Bungarotoxin mRNA along with 50 ng/µl eGFP mRNA. Embryos were then either mounted into a 96-well plate for assaying anaesthesia efficiency or the number of hatched and swimming embryos was scored for developmental stages.

Etomidate solution was prepared as a 10 mg/l solution (7.5 µl of a 4 mg/ml stock solution in DMSO in 3 ml 1x ERM). The DMSO solution was prepared accordingly, yielding a 0.25% DMSO solution. A solution of 1x Tricaine (0.02% w/v, A5040, Sigma- Aldrich) was prepared.

Heart morphology scoring and heart rate measurements

Embryos were imaged for 10 seconds with 25 frames per second in order to score heart morphology and heart rates at 25˚C. The data was imported into R [25] and plotted using ggpubr and xlsx libraries [47].

Startle-response assay

Demounted, with α-Bungarotoxin mRNA injected embryos and control embryos were startled with a pipette tip for 10 times. The number of responses was noted and plotted in R using the ggpubr library.

Fluorescent protein cloning and transcription

All fluorescent proteins were cloned into pGGEV3 from the Golden GateWAY toolkit [48]. Each construct was cloned with a start and stop codon to ensure maximum comparability of the resulting mRNAs. Fluorescent proteins were cloned from present plasmids except for the following. cytoplasmic EKAR (Cerulean-Venus) was a gift from Karel Svoboda (Addgene plasmid # 18679) [49], mRuby2-C1 was a gift from Michael Davidson (Addgene plasmid # 54768) [50], pcDNA3-Clover was a gift from Michael Lin (Addgene plasmid # 40259) [50], pmScar-let-i_C1 was a gift from Dorus Gadella (Addgene plasmid # 85044) [46] and SceGFP was a gift from Sabine Strahl [51] eGFP was codon optimized for medaka by OPTIMIZER [21] resulting in the sequence of OleGFP. OleGFP was synthesized by GeneArt Gene Synthesis (Thermo Fisher). Cloned plasmids were linearized with SpeI prior to transcription and transcribed by mMessage mMachine Sp6 Transcription Kit (Thermo Fisher). Fluorescent protein mRNA was microinjected in equimolar amounts compared to 50 ng/µl eGFP mRNA.

SPIM image acquisition

Medaka embryos were anesthetized with 1x Tricaine or by α-Bungarotoxin mRNA injection and stacks were acquired in a MuVi-SPIM (multiview selective plane illumination microscope) [15,16,52] as described before [53] for the 25x detection setup, with the addition of a 488 nm illumination and a corresponding 525/50 bandpass filter. For the measurements of fluorescence intensity the resulting images were divided by the control channel, masked by the Otsu algorithm [54] and subsequently measured.

The resulting tables were imported into R [25] and fused into one dataset. The measurements were linked to conditions and plotted using ggplot2 [55]. The used R libraries were: data.table [56], zoo [57], ggrepel [58], and ggpubr.

The stacks resulting in Fig 6 were recorded and imported into Fiji [24]. They were transformed with the logarithm due to the varying expression of cell types and autofluorescence of leftover pigments.

Comparison of medaka and *E. coli in vivo* fluorescence intensity

E. coli values were extracted from supplementary material of Balleza et al. [18]. Medaka values were calculated as a mean of all data of one fluorescent protein from 23 to 30 hpf from imaged data and normalized to mRFP1* for red fluorescent proteins, eGFP for green fluorescent proteins and Venus for yellow fluorescent proteins (set to a value of 1.2, according to the *E. coli* value).

Codon usage table driven codon averaging and adaptation index

Codon averaging was performed by OPTIMIZER [21], using the codon usage table, which can be obtained from HIVE-CUTs [59]. Codon adaptation indices of all used sequences were scored by using the seqinr library in R [60] and codon usage tables from HIVE-CUTs [59]. The data was plotted using ggplot2 [55], readr [61], data.table [56], condformat [62] and ggrepel [58].

Semi-automated analysis of anesthesia

One slice of each well was acquired by autofocus (16 steps with a distance of 25 μm, software-based) per timepoint in brightfield with a CFI Plan Achromat UW 2x, N.A. 0.06 objective (Nikon). Illumination was performed for 20 ms at an LED intensity of 100%. The timelapse was recorded for at least 45 hours in 20 or 33 minute intervals. Subsequently the imaged medaka were staged for both used plates and the timepoint 0 was set according to the higher starting stage (stage 28) in order to be able to fuse the plate data. The following steps were performed in Fiji [24]. These images were concatenated to a stack per well. Subsequently the square of the difference of timepoints was calculated and exported as a table.

The resulting tables were loaded into R [25] and fused into one dataset. The negative wells (dead or non-developing embryos) were dropped from the data set, the wells were linked to the corresponding conditions and the data was plotted using ggplot2. The used R libraries were: data.table [56] and ggplot2 [55]. Customized scripts are available through github (https://git.io/fAPnh).

Semi-automated analysis of fluorescent proteins

A total of 12 z-slices with 100 μm step size were acquired with a CFI Plan Fluor 4x, N.A. 0.13 objective (Nikon) per well, guaranteeing the embryo to be included in the image. These slices were acquired in the previously described green and red channel. Illumination was performed for 50 ms at an LED intensity of 50% for both channels. Yellow and green fluorescent proteins were recorded in the green channel due to the limitation of light-sheet microscopes of requiring the according filter. The timelapse was recorded from directly after injection up to at least 40 hours for the longer experiments, once each day for the 2, 3 and 4 dpf experiment and from injection to 48 hours for the codon adaptation experiment. The following steps were performed in Fiji [24]. Each slice of each channel was masked by both channels by applying an auto threshold with the Otsu algorithm and cropping each channel by both resulting masks [54]. The resulting, masked images were measured by excluding the background. All wells were checked for fluorescence at the maximum and the half-maximum timepoint in order to exclude developmentally impaired or dead embryos.

The resulting tables were imported into R [25] and fused into one dataset. The negative wells were discarded, the wells were linked to the corresponding conditions and normalized to the injection control per well at 10 hpf. Used was the data masked by the channel of the injection control to ensure automatic cropping. The data was plotted using ggplot2. The used R

libraries were: data.table [56], zoo [57], ggrepel [58] and ggplot2 [55]. Customized scripts are available through github (https://git.io/fAPnh).

Supporting information

S1 Fig. Wild-type vs. dechorionated fluorescence extraction. Embryos were injected as previously mentioned. Half of each condition was dechorionated. Both conditions were imaged at 2, 3 and 4dpf and compared to each other. Optical properties of the chorion were negligible and therefore neglected in the analysis since dechorionation has a larger impact on development, especially when performed in an early stage (2–4 dpf).
(TIF)

S2 Fig. Codon adaptation indices of all used sequences. Codon adaptation index of each sequence is plotted for medaka and human along with a diagonal line for orientation.
(TIF)

S3 Fig. Injections of α-Bungarotoxin have no detectable impact on heart development. (A) Embryos after demounting from the 96-well plate and finishing the assay (stage 31). No cardiac defects are visible in both controls and embryos injected with α-Bungarotoxin mRNA. For Tricaine, mild defects can be detected, whereas severe defects can be observed in Etomidate treated embryos. (B) Heart rate of α-Bungarotoxin is statistically indistinguishable to its control (mock injection). Mild defects and changes can be observed in Tricaine and Etomidate treated embryos (asterisks indicate P-values: **** $P < = 0.0001$, *** $P < = 0.001$, ** $P < = 0.01$, * $P < = 0.05$, ns $P > 0.05$). (C) Different dilutions of α-Bungarotoxin were tested in order to adjust the concentration so fish would wake up after microscopy. Embryos were injected with 0, 3, 6, 12 or 25 ng/μl α-Bungarotoxin mRNA along with eGFP mRNA as an injection control. The number of hatched embryos and the number of swimming embryos per condition was scored (0 ng/μl: n = 33 fish, 3 ng/μl: n = 34 fish, 6 ng/μl: n = 16 fish, 12 ng/μl: n = 24 fish, 25 ng/μl: n = 22 fish).
(TIF)

S4 Fig. Adult medaka with pigment knockout. Addition to Fig 5B. Adult fish of the wild-type strain, the *oca2*$^{-/-}$ mutant line and the double pigment knockout line were imaged.
(TIF)

S1 Movie. Embryos with different anesthetics. Collection of embryos used in the analysis of Fig 4B. Color code is matching the color code in Fig 4.
(MP4)

S2 Movie. Development of a wild-type and mutant embryo. Development of a wild-type and a *oca2*$^{-/-}$ pigment knockout embryo.
(MP4)

S3 Movie. A developing spooky embryo. Stitched stacks of a developing *spooky* embryo, injected with with *α-Bungarotoxin*, *eGFP* and *mCherry* coupled to *histone2a*. The imaging time was 48 hours and the time interval 1 hour between the stacks.
(AVI)

S1 Table. Fluorescent proteins used in this study. All fluorescent proteins used throughout this work including addgene identifiers for comparisons, sequences and mutations from ancestor fluorescent proteins. Furthermore, fluorescent proteins were compared to the classification in the recent publication of Balleza et al., where they made an effort to distinguish the

different fluorescent protein versions [18].
(XLSX)

S2 Table. All plates analyzed for this study.
(XLSX)

S1 Dataset. Minimal dataset.
(ZIP)

Acknowledgments

Author Contributions

Conceptualization: Colin Q. Lischik, Joachim Wittbrodt.

Data curation: Colin Q. Lischik, Leonie Adelmann.

Formal analysis: Colin Q. Lischik.

Funding acquisition: Joachim Wittbrodt.

Investigation: Colin Q. Lischik, Leonie Adelmann, Joachim Wittbrodt.

Methodology: Colin Q. Lischik, Leonie Adelmann.

Project administration: Colin Q. Lischik, Joachim Wittbrodt.

Resources: Joachim Wittbrodt.

Software: Colin Q. Lischik.

Supervision: Joachim Wittbrodt.

Validation: Colin Q. Lischik.

Visualization: Colin Q. Lischik.

Writing – original draft: Colin Q. Lischik, Joachim Wittbrodt.

Writing – review & editing: Colin Q. Lischik, Joachim Wittbrodt.

References

1. Huisken J, Swoger J, Del Bene F, Wittbrodt J, Stelzer EHK. Optical sectioning deep inside live embryos by selective plane illumination microscopy. Science. 2004; 305: 1007–9. https://doi.org/10.1126/science.1100035 PMID: 15310904

2. Keller PJ, Schmidt AD, Santella A, Khairy K, Bao Z, Wittbrodt J, et al. Fast, high-contrast imaging of animal development with scanned light sheet-based structured-illumination microscopy. Nat Methods. Nature Publishing Group; 2010; 7: 637–642. https://doi.org/10.1038/nmeth.1476 PMID: 20601950

3. Rembold M, Lahiri K, Foulkes NS, Wittbrodt J. Transgenesis in fish: efficient selection of transgenic fish by co-injection with a fluorescent reporter construct. Nat Protoc. 2006; 1: 1133–9. https://doi.org/10.1038/nprot.2006.165 PMID: 17406394

4. Seleit A, Krämer I, Ambrosio E, Stolper JS, Dross N, Lischik CQ, et al. Neural stem cells induce the formation of their physical niche during organogenesis. Elife. 2017; 0: 1–30. http://dx.doi.org/10.1101/149955

5. Kirchmaier S, Naruse K, Wittbrodt J, Loosli F. The Genomic and Genetic Toolbox of the Teleost Medaka (Oryzias latipes). Genetics. 2015; 199: 905–918. https://doi.org/10.1534/genetics.114.173849 PMID: 25855651

6. Driever W, Stemple D, Schier A, Solnica-Krezel L. Zebrafish: genetic tools for studying vertebrate development. Trends Genet. 1994; 10: 152–159. https://doi.org/10.1016/0168-9525(94)90091-4 PMID: 8036717

7. Centanin L, Ander J-J, Hoeckendorf B, Lust K, Kellner T, Kraemer I, et al. Exclusive multipotency and preferential asymmetric divisions in post-embryonic neural stem cells of the fish retina. Development. 2014; 141: 3472–3482. https://doi.org/10.1242/dev.109892 PMID: 25142461

8. Pan YA, Freundlich T, Weissman T a, Schoppik D, Wang XC, Zimmerman S, et al. Zebrabow: multi-spectral cell labeling for cell tracing and lineage analysis in zebrafish. Development. 2013; 140: 2835–46. https://doi.org/10.1242/dev.094631 PMID: 23757414

9. Culver JC, Dickinson ME. The effects of hemodynamic force on embryonic development. Microcirculation. 2010; 17: 164–178. https://doi.org/10.1111/j.1549-8719.2010.00025.x PMID: 20374481

10. Fujii R. The regulation of motile activity in fish chromatophores. Pigment Cell Res. 2000; 13: 300–319. https://doi.org/10.1034/j.1600-0749.2000.130502.x PMID: 11041206

11. Kimura T, Nagao Y, Hashimoto H, Yamamoto-Shiraishi Y, Yamamoto S, Yabe T, et al. Leucophores are similar to xanthophores in their specification and differentiation processes in medaka. Proc Natl Acad Sci U S A. 2014; 111: 7343–8. https://doi.org/10.1073/pnas.1311254111 PMID: 24803434

12. Karlsson J, von Hofsten J, Olsson P-E. Generating Transparent Zebrafish: A Refined Method to Improve Detection of Gene Expression During Embryonic Development. Mar Biotechnol. 2001; 3: 0522–0527. https://doi.org/10.1007/s1012601-0053-4 PMID: 14961324

13. Wakamatsu Y, Pristyazhnyuk S, Kinoshita M, Tanaka M, Ozato K. The see-through medaka: A fish model that is transparent throughout life. PNAS. 2001; 98: 10046–10050. https://doi.org/10.1073/pnas.181204298 PMID: 11526229

14. Ohshima A, Morimura N, Matsumoto C, Hiraga A, Komine R, Kimura T, et al. Effects of Body-Color Mutations on Vitality: An Attempt to Establish Easy-to-Breed See-Through Medaka Strains by Outcrossing. G3. 2013; 3: 1577–1585. https://doi.org/10.1534/g3.113.007575 PMID: 23893740

15. Medeiros G de, Norlin N, Gunther S, Albert M, Panavaite L, Fiuza U-M, et al. Confocal multiview light-sheet microscopy. Nat Commun. Nature Publishing Group; 2015; 6: 8881. https://doi.org/10.1038/ncomms9881 PMID: 26602977

16. Krzic U, Gunther S, Saunders TE, Streichan SJ, Hufnagel L. Multiview light-sheet microscope for rapid in toto imaging. Nat Methods. 2012; 9: 730–733. https://doi.org/10.1038/nmeth.2064 PMID: 22660739

17. Iwamatsu T. Stages of normal development in the medaka Oryzias latipes. Mech Dev. 2004; 121: 605–618. https://doi.org/10.1016/j.mod.2004.03.012 PMID: 15210170

18. Balleza E, Kim JM, Cluzel P. A systematic characterization of maturation kinetics of fluorescent proteins in live cells. Nat Methods. 2017; 6: 1–10. https://doi.org/10.1038/nmeth.4509

19. Heppert JK, Dickinson DJ, Pani AM, Higgins CD, Steward A, Ahringer J, et al. Comparative assessment of fluorescent proteins for in vivo imaging in an animal model system. Strome S, editor. Mol Biol Cell. The American Society for Cell Biology; 2016; 27: 3385–3394. https://doi.org/10.1091/mbc.E16-01-0063 PMID: 27385332

20. Puigbò P, Bravo IG, Garcia-Vallvé S. E-CAI: A novel server to estimate an expected value of Codon Adaptation Index (eCAI). BMC Bioinformatics. 2008; 9: 1–7. https://doi.org/10.1186/1471-2105-9-1

21. Puigbò P, Guzmán E, Romeu A, Garcia-Vallvé S. OPTIMIZER: A web server for optimizing the codon usage of DNA sequences. Nucleic Acids Res. 2007; 35: 126–131. https://doi.org/10.1093/nar/gkm219 PMID: 17439967

22. Kimmel CB, Ballard WW, Kimmel SR, Ullmann B, Schilling TF. Stages of embryonic development of the zebrafish. Dev Dyn an Off public. 1995; 203: 253–310. https://doi.org/10.1002/aja.1002030302 PMID: 8589427

23. Swinburne IA, Mosaliganti KR, Green AA, Megason SG. Improved Long-Term Imaging of Embryos with Genetically Encoded α-Bungarotoxin. PLoS One. 2015; 10: e0134005. https://doi.org/10.1371/journal.pone.0134005 PMID: 26244658

24. Schindelin J, Arganda-Carreras I, Frise E, Kaynig V, Longair M, Pietzsch T, et al. Fiji: An open-source platform for biological-image analysis. Nat Methods. 2012; 9: 676–682. https://doi.org/10.1038/nmeth.2019 PMID: 22743772

25. R Core Team. R: A Language and Environment for Statistical Computing [Internet]. Vienna, Austria; 2018. Available: https://www.r-project.org/

26. Stemmer M, Thumberger T, del Sol Keyer M, Wittbrodt J, Mateo JL. CCTop: An Intuitive, Flexible and Reliable CRISPR/Cas9 Target Prediction Tool. PLoS One. 2015; 10: e0124633. https://doi.org/10.1371/journal.pone.0124633 PMID: 25909470

27. Fukamachi S, Asakawa S, Wakamatsu Y, Shimizu N, Mitani H, Shima A. Conserved function of medaka pink-eyed dilution in melanin synthesis and its divergent transcriptional regulation in gonads among vertebrates. Genetics. 2004; 168: 1519–1527. https://doi.org/10.1534/genetics.104.030494 PMID: 15579703

28. Hidehito I, Yoshitaka B, Akihiko K, Hiroshi H. Expression of the tyrosinase-encoding gene in a colorless melanophore mutant of the medaka fish, Oryzias latipes. Gene. 1994; 150: 319–324. https://doi.org/10.1016/0378-1119(94)90445-6 PMID: 7821799

29. Kimura T, Takehana Y, Naruse K. pnp4a Is the Causal Gene of the Medaka Iridophore Mutant, guanineless. G3. 2017; 7: g3.117.040675. https://doi.org/10.1534/g3.117.040675 PMID: 28258112

30. Wu RS, Lam II, Clay H, Duong D, Deo RC, Coughlin SR. A Rapid Method for Directed Gene Knockout for Screening in G0 Zebrafish. Dev Cell. Elsevier Inc.; 2018; 46: 112–125.e4. https://doi.org/10.1016/j.devcel.2018.06.003 PMID: 29974860

31. Caussinus E, Kanca O, Affolter M. Fluorescent fusion protein knockout mediated by anti-GFP nanobody. Nat Struct Mol Biol. Nature Publishing Group; 2011; 19: 117–121. https://doi.org/10.1038/nsmb.2180 PMID: 22157958

32. Kubala MH, Kovtun O, Alexandrov K, Collins BM. Structural and thermodynamic analysis of the GFP:GFP-nanobody complex. Protein Sci. 2010; 19: 2389–2401. https://doi.org/10.1002/pro.519 PMID: 20945358

33. Kamiyama D, Sekine S, Barsi-Rhyne B, Hu J, Chen B, Gilbert LA, et al. Versatile protein tagging in cells with split fluorescent protein. Nat Commun. Nature Publishing Group; 2016; 7: 11046. https://doi.org/10.1038/ncomms11046 PMID: 26988139

34. Zacharias DA, Violin JD, Newton AC. Partitioning of Lipid-Modified Monomeric CFPs into Membrane Microdomains of Live Cells. Science. 2002; 296: 913–6. https://doi.org/10.1126/science.1068539 PMID: 11988576

35. Katoh Y, Terada M, Nishijima Y, Takei R, Nozaki S, Hamada H, et al. Overall Architecture of the Intraflagellar Transport (IFT)-B Complex Containing Cluap1/IFT38 as an Essential Component of the IFT-B Peripheral Subcomplex. J Biol Chem. 11200 Rockville Pike, Suite 302, Rockville, MD 20852–3110, U.S.A.: American Society for Biochemistry and Molecular Biology; 2016; 291: 10962–10975. https://doi.org/10.1074/jbc.M116.713883 PMID: 26980730

36. Day RN, Davidson MW. The fluorescent protein palette: tools for cellular imaging. Chem Soc Rev. 2009; 38: 2887–2921. https://doi.org/10.1039/b901966a PMID: 19771335

37. Keller PJ, Schmidt AD, Wittbrodt J, Stelzer EHK. Reconstruction of Zebrafish Early Embryonic Development by Scanned Light Sheet Microscopy. Science (80-). 2008; 322: 1065–1069. https://doi.org/10.1126/science.1162493 PMID: 18845710

38. Zeller RW, Weldon DS, Pellatiro MA, Cone AC. Optimized green fluorescent protein variants provide improved single cell resolution of transgene expression in ascidian embryos. Dev Dyn. 2006; 235: 456–467. https://doi.org/10.1002/dvdy.20644 PMID: 16287050

39. Dray N, Bedu S, Vuillemin N, Alunni A, Coolen M, Krecsmarik M, et al. Large-scale live imaging of adult neural stem cells in their endogenous niche. Development. 2015; 142: 3592–3600. https://doi.org/10.1242/dev.123018 PMID: 26395477

40. Readman GD, Owen SF, Knowles TG, Murrell JC. Species specific anaesthetics for fish anaesthesia and euthanasia. Sci Rep. Springer US; 2017; 7: 7102. https://doi.org/10.1038/s41598-017-06917-2 PMID: 28769117

41. Barbosa JS, Sanchez-gonzalez R, Di Giaimo R, Baumgart EV, Theis FJ, Götz M, et al. Live imaging of adult neural stem cell behavior in the intact and injured zebrafish brain. Science. 2015; 348: 789–93. https://doi.org/10.1126/science.aaa2729 PMID: 25977550

42. Frazier DT, Narahashi T. Tricaine (MS-222): Effects on ionic conductances of squid axon membranes. Eur J Pharmacol. 1975; 33: 313–317. https://doi.org/10.1016/0014-2999(75)90175-2 PMID: 171163

43. Reynolds DS, Rosahl TW, Cirone J, O'Meara GF, Haythornthwaite A, Newman RJ, et al. Sedation and Anesthesia Mediated by Distinct GABAA Receptor Isoforms. J Neurosci. 2003; 23: 8608 LP–8617. Available: http://www.jneurosci.org/content/23/24/8608.abstract

44. Koster R, Stick R, Loosli F, Wittbrodt J. Medaka spalt acts as a target gene of hedgehog signaling. Development. 1997; 124: 3147–3156. PMID: 9272955

45. Hwang WY, Fu Y, Reyon D, Maeder ML, Tsai SQ, Sander JD, et al. Efficient genome editing in zebrafish using a CRISPR-Cas system. Nat Biotechnol. Nature Publishing Group, a division of Macmillan Publishers Limited. All Rights Reserved.; 2013; 31: 227. Available: http://dx.doi.org/10.1038/nbt.2501 PMID: 23360964

46. Bindels DS, Haarbosch L, van Weeren L, Postma M, Wiese KE, Mastop M, et al. mScarlet: a bright monomeric red fluorescent protein for cellular imaging. Nat Methods. Nature Publishing Group, a division of Macmillan Publishers Limited. All Rights Reserved.; 2016; 14: 53. Available: http://dx.doi.org/10.1038/nmeth.4074 PMID: 27869816

47. Dragulescu AA. xlsx: Read, write, format Excel 2007 and Excel 97/2000/XP/2003 files [Internet]. 2014. Available: https://cran.r-project.org/package=xlsx

48. Kirchmaier S, Lust K, Wittbrodt J. Golden GATEway Cloning—A Combinatorial Approach to Generate Fusion and Recombination Constructs. PLoS One. 2013; 8: e76117. https://doi.org/10.1371/journal.pone.0076117 PMID: 24116091

49. Harvey CD, Ehrhardt AG, Cellurale C, Zhong H, Yasuda R, Davis RJ, et al. A genetically encoded fluorescent sensor of ERK activity. Proc Natl Acad Sci U S A. 2008; 105: 19264–19269. 0804598105 [pii]\r https://doi.org/10.1073/pnas.0804598105 PMID: 19033456

50. Lam AJ, St-Pierre F, Gong Y, Marshall JD, Cranfill PJ, Baird MA, et al. Improving FRET dynamic range with bright green and red fluorescent proteins. Nat Methods. 2012; 9: 1005–1012. https://doi.org/10.1038/nmeth.2171 PMID: 22961245

51. Xu C, Wang S, Thibault G, Ng DTW. Futile Protein Folding Cycles in the ER Are Terminated by the Unfolded Protein O-Mannosylation Pathway. Science (80-). 2013; 340: 978–982. https://doi.org/10.1126/science.1234055 PMID: 23704572

52. Tomer R, Khairy K, Amat F, Keller PJ. Quantitative high-speed imaging of entire developing embryos with simultaneous multiview light-sheet microscopy. Nat Methods. Nature Publishing Group; 2012; 9: 755–763. https://doi.org/10.1038/nmeth.2062 PMID: 22660741

53. Caroti F, González Avalos E, Noeske V, González Avalos P, Kromm D, Wosch M, et al. Decoupling from yolk sac is required for extraembryonic tissue spreading in the scuttle fly Megaselia abdita. Elife. 2018; 7: 1–19. https://doi.org/10.7554/eLife.34616 PMID: 30375972

54. Otsu N. A threshold selection method from gray level histograms. {IEEE} Trans Syst Man Cybern. 1979; 9: 62–66.

55. Wickham H. ggplot2: Elegant Graphics for Data Analysis [Internet]. Springer-Verlag New York; 2009. Available: http://ggplot2.org

56. Dowle M, Srinivasan A. data.table: Extension of 'data.frame'[Internet]. 2017. Available: https://cran.r-project.org/package=data.table

57. Zeileis A, Grothendieck G. zoo: S3 Infrastructure for Regular and Irregular Time Series. J Stat Softw. 2005; 14: 1–27. https://doi.org/10.18637/jss.v014.i06

58. Slowikowski K. ggrepel: Repulsive Text and Label Geoms for "ggplot2" [Internet]. 2017. Available: https://cran.r-project.org/package=ggrepel

59. Athey J, Alexaki A, Osipova E, Rostovtsev A, Santana-Quintero L V., Katneni U, et al. A new and updated resource for codon usage tables. BMC Bioinformatics. BMC Bioinformatics; 2017; 18: 1–10. https://doi.org/10.1186/s12859-016-1414-x

60. Charif D, Lobry JR. Seqin{R} 1.0–2: a contributed package to the {R} project for statistical computing devoted to biological sequences retrieval and analysis. In: Bastolla U, Porto M, Roman HE, Vendruscolo M, editors. Structural approaches to sequence evolution: Molecules, networks, populations. New York: Springer Verlag; 2007. pp. 207–232.

61. Wickham H, Hester J, Francois R. readr: Read Rectangular Text Data [Internet]. 2017. Available: https://cran.r-project.org/package=readr

62. Oller Moreno S. condformat: Conditional Formatting in Data Frames [Internet]. 2017. Available: https://cran.r-project.org/package=condformat